Mechanics of Advanced Composite Structures

Journal homepage: https://macs.semnan.ac.ir/

Semnan University

ISSN: 2423-7043

Research Article

Structural Evaluation of a Horizontal Axis Wind Turbine Composite Blade Using a Monitored Testing Bench

Omar Rajad [a*,b,c], **Youssef Idihya** [b], **Hamid Mounir** [b], **Mohamed Rich** [a], **Ikram Outla** [d]

(a)-LRPSI, Polydisciplinary Faculty, Sultan Moulay Slimane University, Beni Mellal, Morocco
(b)-EMISys Research Team, E3S Research Center, Mohammadia School of Engineers, Mohammed V University in Rabat, Morocco
(c)- Multidisciplinary Laboratory of Exact and Applied Sciences, Superior School of Technology, Fkih Ben Saleh, Morocco
(d)-Alkhalil Center, Private laboratory of Engineering Energy, Beni Mellal, Morocco

ARTICLE INFO

Article history:

Received: 20/08/2025
Revised:
Accepted:

Keywords:

Wind turbine blade;
Bench test;
Stiffness;
Flapwise direction;
Glass Fiber.

ABSTRACT

Accurate prediction of blade fatigue behavior remains a critical challenge in wind energy applications. This study presents a comprehensive evaluation of the mechanical performance of a segmented 3D-printed composite prototype blade. To assess its stiffness characteristics, the blade was subjected to systematically applied load levels in the flapwise direction. The experimental campaign enabled detailed characterization of the blade's stiffness and the initiation and evolution of damage as a function of applied loading and the number of fatigue cycles. A statistical analysis was performed to quantify the uncertainty and repeatability of the measured results. A specialized test bench was designed and constructed to accommodate fatigue testing of blades measuring 712 mm in length. The blade was subjected to controlled cyclic loading while its mechanical response was continuously monitored using a high-resolution imaging system. The collected data revealed a significant increase in total deformation energy of 77.5%, particularly near the root (point 1), and a corresponding decrease in stiffness of 77% after cyclic loading in the flapwise direction. These results provide critical insights into the blade's structural health and dynamic response during service and have informed improvements in the manufacturing process to ensure that the final products meet stringent reliability and safety standards under severe operating conditions. The study was further evaluated by testing two blades with identical geometry and material properties, demonstrating that the derived results were accurate within an error margin not exceeding 10%.

1. Introduction

1.1. Background

Wind energy has emerged as one of the leading sustainable resources in the global transition toward renewable energy. In recent years, significant attention has been devoted to the research and development of sustainable energy technologies [1–4], particularly wind and marine turbines, in response to growing concerns about global climate change and carbon emissions. Wind energy, which leverages aerodynamic principles to harness natural wind flow for electrical power generation, plays a critical role in diversifying global energy portfolios and enhancing energy security.

*** Corresponding author.**
E-mail address: *omatr.rajad@usms.ma*

Cite this article as:
Omar Rajad et al., 2026. Structural evaluation of a horizontal axis wind turbine composite blade using a monitored testing bench. *Mechanics of Advanced Composite Structures*, 13(1), pp. xxx-xxx.

The manufacturing of high-performance composite blades represents a pivotal challenge in the wind energy sector, as blade certification for industrial production depends heavily on manufacturing precision, material reliability, and overall quality assurance [5–7]. Composite materials, valued for their superior strength-to-weight ratio and excellent fatigue resistance, are essential for achieving the mechanical performance required for long-term service under harsh environmental conditions.

During the pre-industrialization phase, rigorous mechanical testing of composite blade structures is essential to verify their strength under both static and dynamic loading conditions. Such tests aim to evaluate stiffness degradation under repetitive loading cycles and to predict the blades' service life. Mechanical testing provides a comprehensive characterization of composite material behavior, assesses structural reliability, and supports improvements in blade design and overall aerodynamic performance, as emphasized by several researchers [6, 8].

Full-scale mechanical testing before blade industrialization is a critical accreditation step for wind turbine blades and plays a crucial role in ensuring long-term reliability [6, 9]. As the primary energy-harvesting components, blades must exhibit a low mass moment of inertia to react quickly to changing wind conditions [10, 11]. Horizontal-axis wind turbine (HAWT) blades, in particular [12], must endure harsh operational conditions, cyclic fatigue loads, and extreme gust events over a designed lifespan of at least 20 years [13, 14]. However, operational challenges remain: blades often experience catastrophic failures under extreme wind loads, such as those encountered during typhoons [15], highlighting the urgent need for continued advancements in design, materials, and durability testing.

1.2. Review of structural studies on composite material enhancement for HAWT blades

Studies on the strength and stiffness assessment of composite blades need to be thoroughly investigated to ensure high durability and safety. Quasi-static damage evaluation and predictive modeling of composite behavior are increasingly employed to enhance the stiffness and overall durability of wind turbine blades. For example, Xiao Chen et al. [16] analyzed the mechanical response of trailing edges and proposed reinforcement strategies to improve load-carrying capacity and buckling resistance. In a related study [17], potential damage modes, such as delamination in spar cap laminates, were experimentally identified as precursors to catastrophic blade failures. These investigations emphasized the significant influence of through-thickness stresses and provided actionable insights to improve design standards for large composite structures.

In another approach, CFD studies have been conducted to apply realistic aerodynamic loads to composite blade structures, and results related to strength and stiffness assessments have been reported [18–24], based on several models proposed by the authors [25].

Furthermore, the post-buckling behavior and failure mechanisms of wind turbine subcomponents have been extensively studied to understand the influence of structural nonlinearities, contact interactions, and progressive material damage [26–28]. Sub-modelling approaches [29, 30] have been applied to gain a detailed understanding of localized failures, contributing to enhanced design robustness and improved damage tolerance.

Additive manufacturing (AM), or 3D printing [31–33], has also shown promising applications in the fabrication of complex parts and assemblies for wind and tidal turbines. AM enables rapid prototyping, allowing engineers and researchers to examine and refine designs prior to full-scale production. This technology, widely adopted in aerospace [34, 35] and hydro-turbine development [36], supports the production of aerodynamic models and prototype blades with reduced costs, minimized material waste, and increased manufacturing flexibility. Optimization studies [37, 38] have demonstrated that AM can significantly enhance the feasibility of producing small and medium-scale wind turbine blades [39, 40], thereby facilitating broader deployment of renewable energy technologies.

The blade examined in this study is based on

the configuration adopted by Kam et al. [41] and complies with internationally recognized standards such as IEC 61400-1 [42] and the Germanischer Lloyd (GL321)

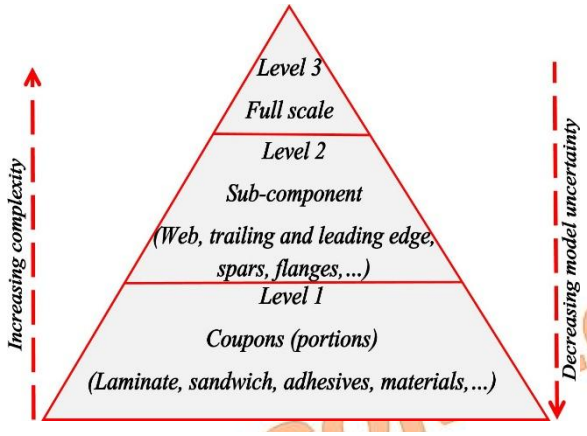

Fig. 1:Sizing Methodologies levels for wind blades testing

guidelines [43]. These standards define critical requirements related to blade tip clearance, material stress and strain limits, and resistance to critical buckling under worst-case loading scenarios. The stiffness design criterion is defined as the ability to resist deformation under anticipated aerodynamic and gravitational loads with minimal flexural displacement, which is a fundamental prerequisite for maintaining aerodynamic efficiency and structural reliability throughout the turbine's operational life.

In compliance with certification protocols, various scaled tests (as illustrated in Fig. 1) are conducted to evaluate the influence of parameters such as fiber type, laminate stacking sequence, number of cycles, loading speeds, and local reinforcement strategies [42, 44, 45].

1.3. Aim of the present study

This manuscript presents a detailed investigation into the stiffness performance and damage progression of a composite wind turbine blade under cyclic flapwise loading. A custom-designed fatigue test bench has been developed in our laboratory to mechanically evaluate the stiffness and fatigue performance of a 712 mm blade prototype. The primary objective is to characterize the evolution of stiffness degradation under cyclic loading, identify critical damage mechanisms, and propose reinforcement strategies to enhance structural health under severe fatigue conditions. Building on previous experimental research, this study emphasizes the optimization of blade design through strategic reinforcement of vulnerable regions, adaptation of fiber materials, and structural reconfiguration by integrating an uncertainty/repeatability study in order to obtain accurate results. Furthermore, similitude laws [46] are applied to extrapolate the experimental findings and predict the behavior of full-scale wind turbine blades, taking into account scaling effects associated with larger rotor diameters.

2. Materials and methods

The process of designing and fabricating the composite wind turbine blade, including the integration of a shear web (rib), is detailed in this section.

The aerodynamic characteristics of the NACA profile selected for this study are illustrated in Fig. 2-(b), with the corresponding aerodynamic performance parameters, such as the lift-to-drag ratio and moment coefficient, plotted as functions of the angle of attack (see Figs. 2-(a) and 2-(c)). The overall three-dimensional surface design of the blade is presented in Fig. 3, based on data from previous studies [41, 47].

The NACA airfoil, originally developed for aircraft wing design, is widely used in wind turbine blade development due to its

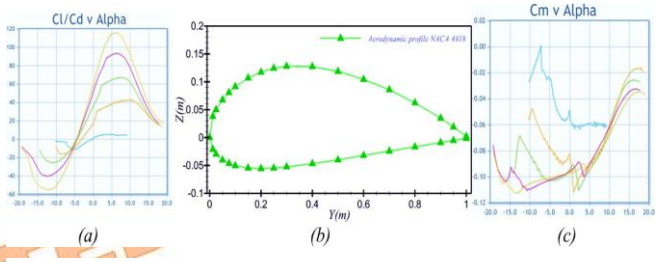

Fig. 2: Aerodynamic specifications of the used profile [47]

favorable aerodynamic properties. By exploiting pressure differentials across the blade surface, the NACA profile facilitates the generation of lift, which translates into the rotational torque required to drive the turbine rotor. The selection of the airfoil shape critically impacts both the aerodynamic efficiency and the mechanical loading experienced by the blade during operation.

In this study, the blade design and structural

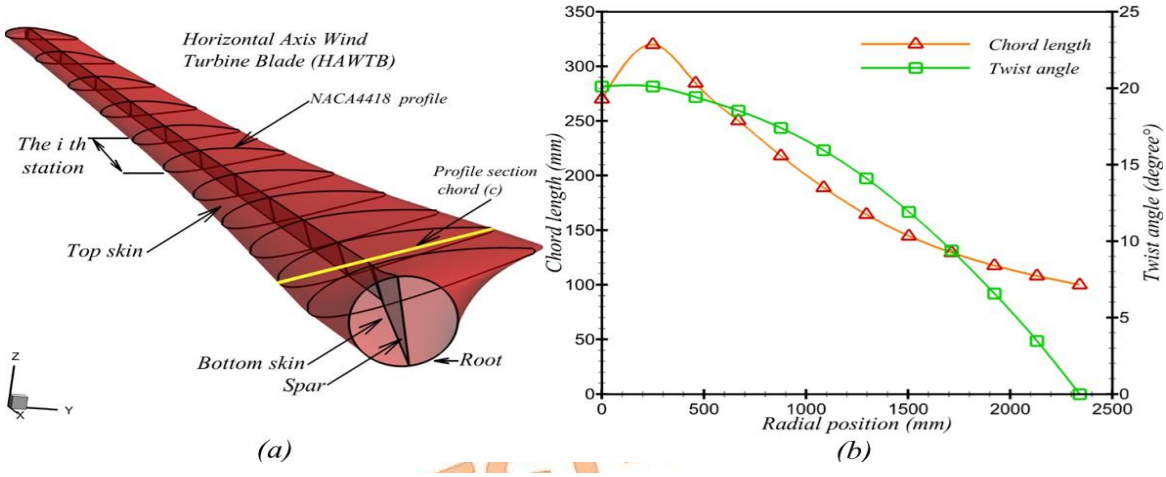

Fig. 3: Wind turbine blade internal and external structural profile

specifications are adapted from the work of Kam et al. [41, 48]. Their research provides a robust foundation for developing a scaled prototype suitable for experimental fatigue and stiffness characterization.

The prototype blade fabricated for this investigation has a total length of 712 mm. Additive manufacturing, specifically 3D printing, was employed to create the blade shell, providing a supportive structure capable of withstanding localized deformations under flexural and cyclic loading conditions. To be precise, a suspended mass of 5 kg is positioned at 0.77*R near the blade tip, in order to measure the deflection at the tip using a laser displacement sensor with 0.48 span ratio, 48% of the total blade length measured from the root as the fixed end, R denotes the radius of the wind turbine rotor, or equivalently the blade length. Thus, the motor was operated at an approximate rotational speed of 290 rad/s. During fatigue tests, the load applied via the slider on the test bench was maintained at a constant magnitude of 48.3 N. All key experimental parameters are summarized in Table 1.

Typically, large-scale blades incorporate internal reinforcements such as ribs or shear webs, designed to enhance structural rigidity and prevent local instabilities such as buckling or delamination. For simplicity and due to laboratory space constraints, the blade coque (outer shell) in this study is reinforced by a simplified internal structure made of 3D-printed polyethylene (PLE) material. Although more complex shear web geometries could be employed, the printed structure offers sufficient mechanical stiffness for the purposes of this scaled experimental campaign. The choice of the 712 mm blade length is justified by the spatial limitations of the custom-built test bench, which necessitated downscaling from the original 2.5-meter blade analyzed by [41].

Table 1: Summary of key experimental parameters

Parameter	Value
Number of specimens	2 blades
Magnitude of the force of measurement	5 kg
Applied load	48.3 N
Suspended mass position	0.77 R (near blade tip)
Span ratio	0.48 (48% of total blade length from root)
Rotor radius (R)	Blade length
Loading frequency	290 rad/s
Number of cycles	> 120,000
Measurement method	Laser displacement sensor at the blade tip

A geometric scale factor of approximately λ=0.28=712/2500 was applied, with an additional part at the cylindrical root section to ensure secure fixation of the composite structure during loading. Notably, dynamic similarity analysis needs to be explicitly investigated to interpret across different blade scales. To be precise, the blade prototype was manufactured at a geometric scale factor of λ = 0.28, which requires consideration of similitude principles to interpret the structural and dynamic behavior. Under the assumption that material properties are identical between the scaled model and the full-size blade, all geometric dimensions scale linearly with λ,

while cross-sectional areas and volumes scale with λ_2 and λ_3, respectively. Because bending behavior dominates for cantilevered wind-turbine blades, the flexural rigidity scales with λ_4, leading the scaled model to exhibit significantly reduced stiffness compared to the prototype. Similarly, the mass and rotational inertia scale with λ_3 and λ_5, which directly affect the dynamic response. As a consequence, the natural bending frequencies scale inversely with geometry, yielding $f_m = f_p/\lambda$, meaning that the 0.28-scale blade vibrates at approximately 3.6 times the frequency of the full-scale blade. To maintain stress similitude during testing, the applied bending moment and corresponding tip load must scale with $\lambda 3$, whereas the resulting deflections scale linearly with λ. These similarity relations provide the theoretical basis for interpreting stiffness, load levels, and dynamic response in the reduced-scale experimental model.

Under the assumptions, the elastic behavior of the blade subjected to wind loads could be presented using these scaling laws :

- **Geometry scaling**

Length: $L_m = \lambda L_p$ (1)

Cross-sectional : $A_m = \lambda^2 A_p$ (2)

ss : $\begin{cases} Vm = \lambda^3 Vp \\ Mm = \rho Vm = \lambda^3 mp \end{cases}$ (3)

- **Bending stiffness scaling**

Second moment of area: (4)

$I_m = \lambda^4 I_p$

Flexural rigidity: (5)

$(EI)m = E\ Im = \lambda^4 (EI)p$

Structural stiffness

$km \approx (EI)_m / Lm^3$ (6)
$= \lambda\ k_p$

Tip deflection under a concentrated load

$\delta_m = (P_m L_m^3) / (C (EI)_m)$ (7)
$\delta_m = \lambda\ \delta_p$ (8)

The total deformation energy U quantifies the elastic energy stored in the blade structure under applied loads and serves as an indicator of stiffness and structural integrity. For a linear elastic structure, where the load F is proportional to the displacement δ (valid for small deformations and within the material's linear range), the total deformation energy can be expressed as:

$$U = \frac{1}{2} F\delta \qquad (9)$$

This expression assumes a triangular load–displacement response, corresponding to a single load application without significant damage or geometric nonlinearities. It is particularly suitable for the preliminary evaluation of stiffness in small-scale blade prototypes made of composite materials with linear elastic behavior.

For nonlinear structures, where the load–displacement relationship is not proportional due to material nonlinearity (e.g., matrix cracking, fiber-matrix debonding) or geometric effects (large deformations), the total deformation energy must be computed as the area under the actual load–displacement curve:

$$U = \int_0^{\delta} F(\tilde{\delta})\, d\tilde{\delta} \qquad (10)$$

Here, $F(\tilde{\delta})$ (Eq. 10) represents the instantaneous load at the displacement $\tilde{\delta}$. This formulation captures the progressive energy absorption and stiffness degradation in the blade structure, making it suitable for fatigue studies and the evaluation of damage accumulation in composite wind turbine blades.

By comparing the linear and nonlinear formulations, one can assess the range of validity of the linear approximation and quantify additional energy dissipation due to nonlinear effects, providing a comprehensive understanding of the blade's structural performance.

Figs. 4, 5, and 6 present images of the wind turbine blade rib fabricated using 3D printing with polyethylene material before adding the laminate stacking. This internal

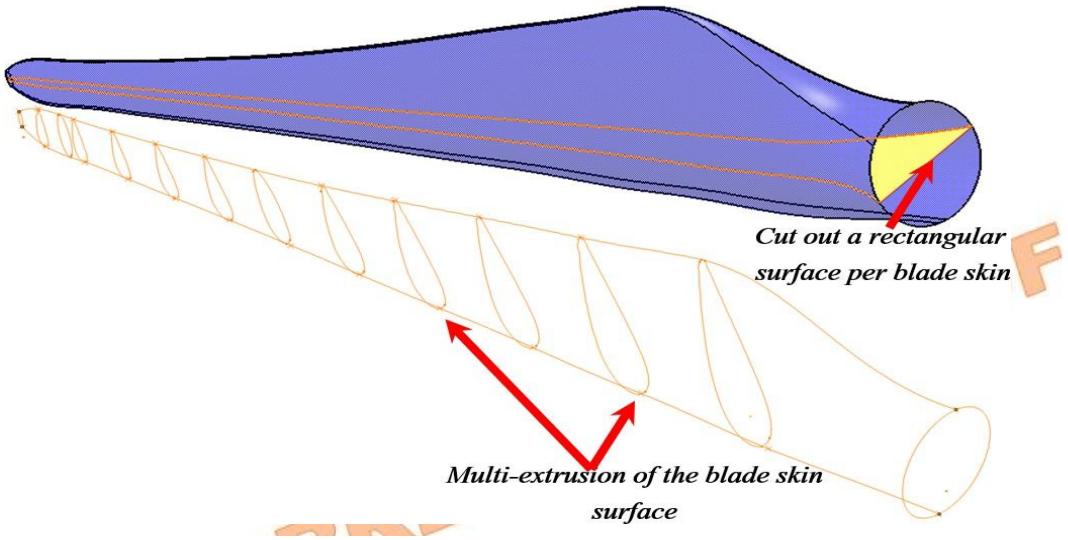

Fig. 4: Surface design of the blade under CATIA V5

structure acts as the shear web, which is crucial for resisting flexural and torsional loads. By significantly increasing the blade's second moment of area (quadratic moment of inertia), the spar enhances global stiffness, delays the onset of local buckling, and mitigates delamination failures in the laminated skin layers [49].

The integration of a robust shear web is essential for maintaining blade stability and structural robustness under operational loads, particularly during extreme wind events where cyclic and dynamic stresses are amplified. By improving stiffness and distributing internal stresses more effectively, the blade's fatigue life and overall durability are considerably enhanced, an indispensable feature for ensuring the long-term reliability of wind turbine systems.

Fig. 5 depicts the overall steps of the manufacturing of the blade prototype with woven carbon and UD glass fiber. Table 2 presents the laminate used in blade skin fabrication.

2.1. Experimental rig

In this study, a custom-designed fatigue test machine was employed to identify the stiffness, strength, and damage progression of a composite blade prototype. Fig. 8 illustrates the experimental setup developed for testing the blade under controlled cyclic loading conditions as depicted in Fig. 7. This paper presents the detailed procedures of the experimental campaign and discusses the obtained results with respect to the mechanical strength and flexural rigidity of the blade.

Regarding the validation of the experimental setup, our work was based on two references. The scaled blade design was carried out based on the literature [28] and our previous work [41]. In these studies, the authors validated the physical model by comparing FEM results with experimental investigations [41]. Thus, the present work involved several experimental investigations to evaluate blade stiffness and strength. Indeed, our study focused exclusively on the experimental design, calibration, and characterization of the test bench. Numerical simulations were cited only to contextualize the state of the art and were not part of our methodological framework. Since the scope of the paper is strictly experimental, numerical–experimental validation falls outside our objectives. The primary objective of this study was to develop a reliable experimental strategy to assess the material capacity and endurance of composite blades under fatigue loading. Various parameters were considered in this investigation, including structural reinforcement configurations, the use of natural fiber composites, and the evaluation of different laminate architectures and manufacturing methods.

The experimental setup consisted of several key components. A 1.4 kW three-phase electrical motor was employed to ensure controlled input shaft speed. A mechanical reducer with a 1/34 ratio was used to significantly increase the output torque, thereby ensuring sufficient flexural loading on the blade structure. The input rotational speed could be varied across five discrete

levels, allowing a wide range of cyclic loading frequencies to be explored. An adjustable eccentric mechanism was integrated into the system to modify the magnitude of the flexural bending moment applied to the blade.

The kinematic diagram of the system demonstrates how the driving torque was converted into an oscillatory force, thereby imposing cyclic bending loads on the blade specimen. Furthermore, the rigidity of the composite blade could be modulated by attaching different suspended masses at varying radial positions along the blade span, thus simulating different loading scenarios.

Table 2: Material specification of the laminate

Parameter	Symbol / Unit	Specifications
Stacking sequence 1 (0.4R from root)	–	[45C / 0G / 90G / 0G / 45C]s
Stacking sequence 2 (all blades)	–	[45C / 45C]s
Fiber orientations	deg	45° (carbon), 0° and 90° (glass)
Resin type	–	Epoxy resin
Fiber volume fraction	Vf (%)	48–52

It is important to note that the experimental setup incorporated several sources of uncertainty that must be accounted for in the fatigue analysis. The test bench was composed of multiple mechanical subassemblies, including blade locking mechanisms, blade supports for load application, and the power transmission system. Mechanical inefficiencies, such as friction losses and localized deformations at material–steel interfaces, were inherent due to differences in hardness and mechanical properties of the contacting materials, as shown in Fig. 5.

In practice, the prototype was manufactured based on a 3D plastic model of the blade, which was designed to act as the blade rib. A sequence of laminate layers was then incorporated to form the bottom and top skins, ensuring adhesion between the two skin parts using adhesive bonding lines. The blade fabrication process was challenging due to the thin shell-shaped structure and the complexity of both external and internal geometries. In addition, during fabrication, particular attention was given to joint interfaces, where local stress concentrations were considered in order to accurately represent the response of continuous composite blades. Consequently, the segmentation of the assembly has only a secondary influence on the global stiffness and fatigue behavior. First, the bonding technique produced quasi-monolithic connections, minimizing stress concentrations and ensuring continuous load transfer. Second, the prototype structure has a relatively limited length.

On the other hand, the mechanical role of the 3D-printed components is primarily to serve as a means to the overall mechanical response by maintaining the geometric integrity of the assembly and by locally constraining the deformation of the composite structure.

The global load transfer is ensured mainly by the composite laminate, while the 3D-printed segments' contribution is secondary but non-negligible, particularly in regions subjected to local bending or shear.

Segmentation of the 3D-printed parts and their subsequent bonding may influence the mechanical response in two ways. First, segmentation introduces interfaces that can locally reduce stiffness due to imperfect continuity and stress redistribution at bonded joints. Second, under cyclic loading, these interfaces may act as preferential sites for damage initiation, potentially affecting fatigue life through interfacial debonding or localized strain concentrations.

The manufacturing process differs fundamentally from real industrial blade fabrication processes (vacuum infusion, hand lay-up, RTM). Such segmented assembly introduces joint interfaces and stress concentrations that could locally reduce stiffness and deviate from the response of continuous composite blades.

To mitigate slippage and enhance adhesion at contact surfaces, the blade clamping surfaces were roughened, and a flexible, soft wood interface was used to ensure secure and damage-free blade fixation.

Fig. 5: Flowchart of Blade Prototype Manufacturing

In addition, manufacturing imperfections and assembly tolerances associated with both the experimental setup and the blade prototype were carefully considered in the analysis. Despite these factors, the overall sensitivity estimation of the setup uncertainties was evaluated and did not exceed 10%, a margin that was acceptable and provides a high level of confidence in the accuracy of the experimental results and subsequent conclusions. Notably, the statistical analyses were conducted to ensure this margin.

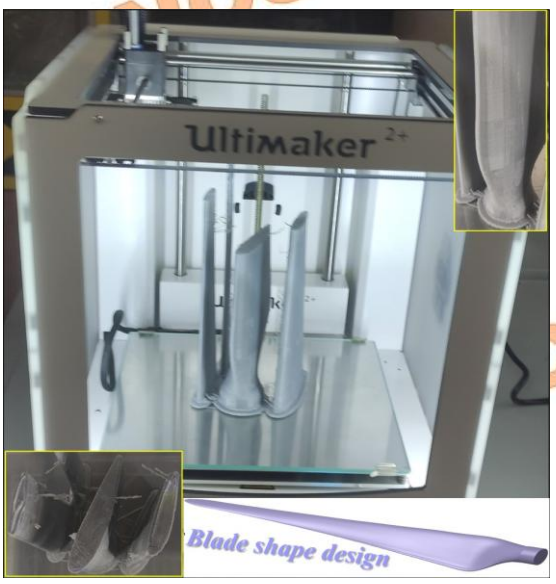

Fig. 6: Additive manufacturing setup, Ultimaker employed in the fabrication of the 3D-printed wind turbine blade rib

Fig. 8 presents the design of the test bench used in this study. The blade structure was clamped at the root, while fatigue loads were applied to its outer surface in the flapwise direction. The loading mechanism consisted of an electrical motor coupled with a crank-rod system.

2.2. Experimental investigations

The primary objective of this experimental investigation was to monitor and characterize the evolution of the flexural rigidity (expressed in N/mm) of a full-scale composite blade prototype under cyclic loading, applied in the flapwise direction. The experimental methodology consisted of systematically applying a suspended mass at various spanwise locations on the blade to induce flexural deformations in two principal orthogonal loading directions.

By conducting a series of controlled fatigue tests with varying numbers of load cycles, the degradation of stiffness over time was assessed, providing valuable insight into the progressive damage mechanisms within the composite structure. Furthermore, this study sought to identify the ultimate load capacity of the blade, defined as the maximum load it can withstand before catastrophic failure, thereby offering a quantitative evaluation of the blade's material strength and overall structural stability.

In addition to stiffness and strength evaluation, a key objective of the post-processing phase was to predict the damage tolerance of the composite blade. Post-

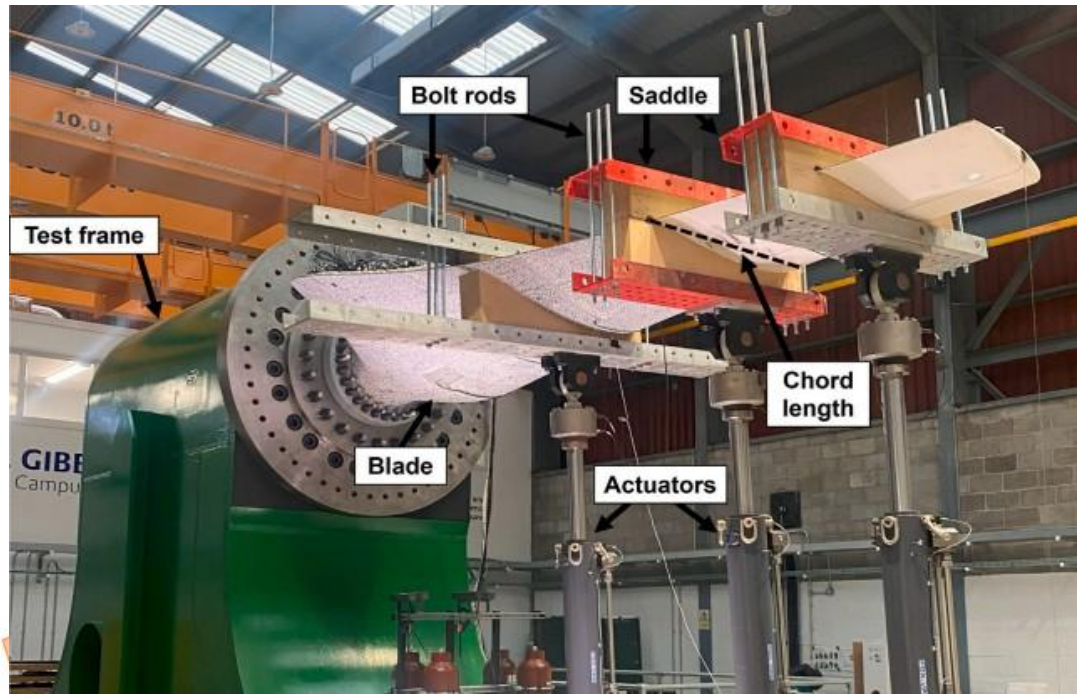

Fig. 7: Experimental configuration for high-load fatigue testing of the blade, featuring multiple saddles securely clamped to the structure [50]

processing of the experimental data involved several critical steps:

- Extraction and smoothing of load–displacement curves at different stages of fatigue life.
- Calculation of stiffness degradation trends as a function of the number of cycles.
- Determination of critical thresholds, such as the first observable stiffness reduction and the onset of nonlinear behavior indicative of internal damage.
- Statistical analysis of scatter in the experimental results, accounting for uncertainties and measurement noise.
- Estimation of residual strength after predefined fatigue intervals to assess the blade's endurance capabilities.
- Damage modeling by correlating stiffness loss with damage initiation and propagation mechanisms, including matrix crushing and cracking, fiber–matrix debonding, and delamination phenomena.

The overall experimental and post-processing strategy thus aimed to establish a comprehensive fatigue performance envelope for the blade, ultimately supporting the development of design improvements, enhanced predictive maintenance strategies, and more reliable service life estimations for wind turbine blades operating under complex loading conditions.

As a matter of fact, to ensure a high level of accuracy and reliability in the experimental results, a comprehensive uncertainty and repeatability analysis was carried out for all measured quantities. Each test configuration was repeated twice using two blade prototypes manufactured with identical materials and processing conditions, allowing an evaluation of the repeatability of key parameters such as stiffness, deflection, and cyclic response. Based on several publications from the literature, such as [51–53], the mean value of each measured quantity was calculated according to Eq. (10), while the statistical dispersion between repeated measurements was quantified using the sample standard deviation in Eq. (11).

Table 3: Test Matrix for Fatigue Testing of Blade Specimens

Speci-men	Amplitude (N)	Frequency (rad/s)	R-Ratio	Max Number of Cycles
S1	48.3	290	0.75	1.2×10^5
S2	48.3	290	0.75	1.2×10^5

Fig. 8: 3D design of the test rig generated in CATIA V5, illustrating its components and configuration.

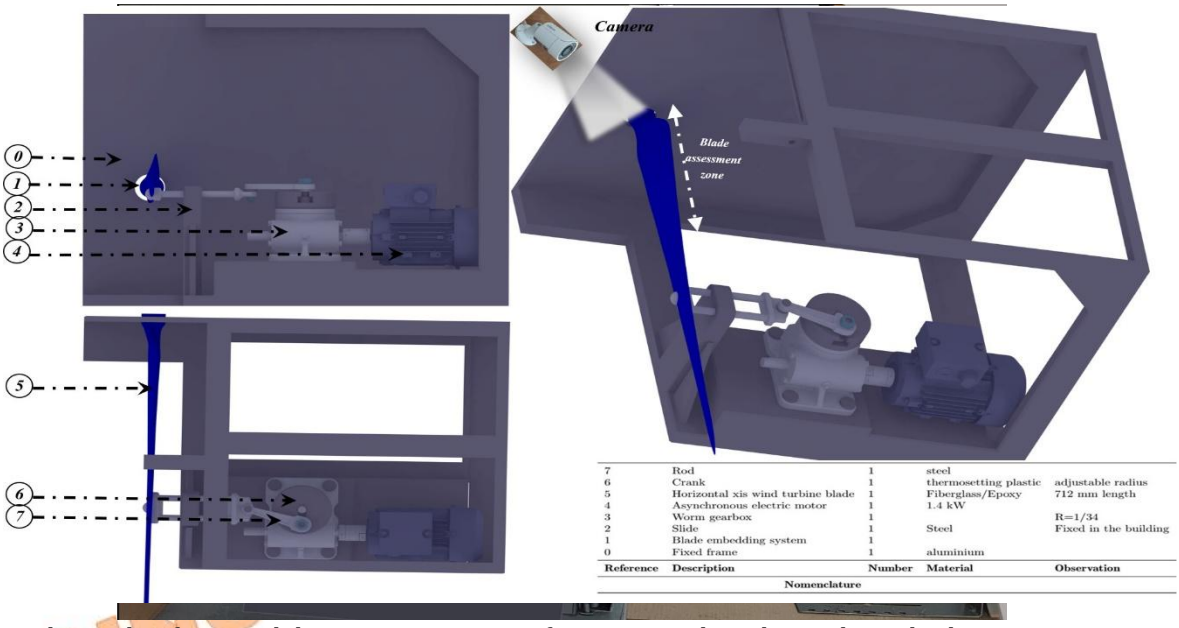

Reference	Description	Number	Material	Observation
Nomenclature				
7	Rod	1	steel	
6	Crank	1	thermosetting plastic	adjustable radius
5	Horizontal xis wind turbine blade	1	Fiberglass/Epoxy	712 mm length
4	Asynchronous electric motor	1	1.4 kW	
3	Worm gearbox	1		R=1/34
2	Slide	1	Steel	Fixed in the building
1	Blade embedding system	1		
0	Fixed frame	1	aluminium	

The study of repeatability is a component of the measurement uncertainty (Type A), which was then obtained from Eq. (12). Type B uncertainties, derived from the calibration data of the instrumentation (suspended masses, displacement sensor, and data acquisition system), were also included in the analysis. For quantities derived from multiple measured inputs, such as stiffness calculated as k = P /δ, the combined uncertainty was evaluated using the law of propagation of uncertainty given for uncorrelated inputs in Eq. (13a) and for correlated inputs in Eq. (13b). The combined standard uncertainty for each parameter was obtained through the root-sum-square method. Reporting results as mean combined uncertainty, along with error bars in the figures, provides a transparent and rigorous assessment of the accuracy and reliability of the experimental campaign. The mean value could be expressed as

$$\bar{x} = \frac{1}{n}\sum_{i=1}^{n} x_i \qquad (10)$$

The sample standard deviation is expressed:

$$s = \sqrt{\frac{1}{n-1}\sum_{i=1}^{n}(x_i - \bar{x})^2} \qquad (11)$$

Type-A standard uncertainty could be expressed as :

$$u_A = \frac{s}{\sqrt{n}} \qquad (12)$$

Thus, the total standard uncertainty:

$$u_c = \sqrt{u_A^2 + u_B^2} \qquad (13c)$$

Propagation of uncertainty (uncorrelated inputs) is stated as :

$$u_y = \sqrt{\sum_{i=1}^{m}\left(\frac{\partial f}{\partial x_i}\right)^2 u_{x_i}^2} \qquad (13a)$$

Propagation of uncertainty (correlated inputs) could be declared as :

$$u_y = \sqrt{\sum_{i=1}^{m}\sum_{j=1}^{m}\frac{\partial f}{\partial x_i}\frac{\partial f}{\partial x_j}\,cov(x_i, x_j)} \qquad (13b)$$

Coefficient of variation (CV): The coefficient of variation was computed to evaluate the relative dispersion of the measurements, Eq. (14):

$$CV = \frac{s}{\bar{x}} \times 100\% \qquad (14)$$

This study introduces several novel contributions relative to previous experimental works, including our earlier publications. It provides a thorough fatigue characterization of a scaled composite blade prototype subjected to cyclic flapwise loading, featuring high-resolution monitoring of local damage and stiffness

Fig. 9: Experimental test bench designed to measure the stiffness of the blade structure under controlled loading conditions

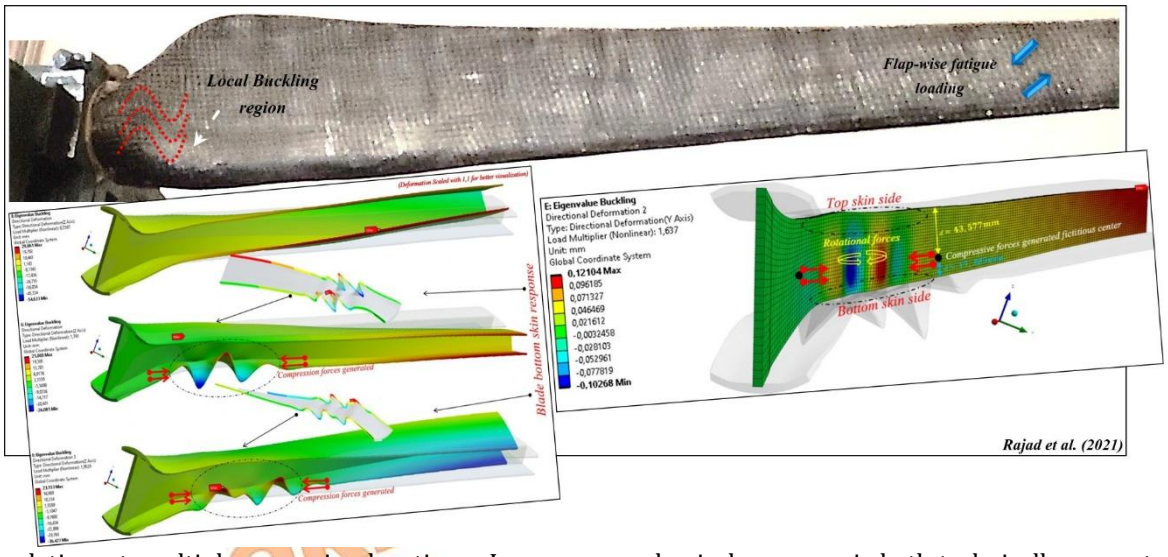

degradation at multiple spanwise locations. In addition, the research establishes a direct relationship between stiffness reduction and total deformation energy with specific damage mechanisms, such as matrix cracking, delamination, and fiber breakage, offering new insights into progressive damage accumulation in segmented composite blades. A rigorous statistical study, including the propagation of measurement uncertainties for stiffness, was also performed to ensure that the observed fatigue behavior accurately reflects the structural response rather than experimental noise. Furthermore, the study evaluates the mechanical role of 3D-printed internal supports, revealing their indirect contribution to global stiffness and fatigue performance, which has not been addressed in prior experimental investigations. Collectively, these aspects provide a comprehensive and novel experimental framework for understanding the fatigue behavior and structural performance of segmented composite blades under cyclic loading.

Fig. 10: Observation of local buckling patterns and structural deformations under cyclic loading and following its composite

3. Results and discussions

The structural performance of the wind blade prototypes was rigorously assessed, and two complementary analyses were carried out. First, experimental evaluations of blade stiffness focused on quantifying the flexural response at different locations along the span under controlled cyclic loading, providing insight into stiffness degradation and fatigue behavior. Second, the uncertainty and repeatability analysis examined the reliability of the measured data by evaluating statistical dispersion, measurement uncertainty, and consistency between the two blade prototypes. As a whole, these sections ensure that the reported mechanical response is both technically accurate and supported by an appropriate assessment of measurement quality.

3.1. Experimental evaluations of blade structure

Our experimental results were presented and analyzed based on the dynamic testing of a composite blade structure subjected to extreme cyclic loading in the flapwise direction. The primary objective of these tests was to predict and characterize the failure mechanisms observed during fatigue and to discuss damage propagation and the increase in total deformation energy of the structure. To be precise, the total deformation energy is the work done by internal stresses throughout a deformable solid during loading. It represents the energy stored in the material due to nonlinear deformation, including contributions from axial, bending, shear, and torsional strains. For instance, fiber breakage, delamination, matrix cracking, and matrix crushing are among the most common damage mechanisms that can be found in such composite structures. The structural response was notably nonlinear and elastic due to the structure's length and was influenced by geometric, material, and contact nonlinearities, as detailed in [28]. The stiffness of the blade was evaluated by suspending calibrated masses at various points and measuring the resulting maximum deflection. Indeed, our enhanced experimental procedure depicts a strategy adopted to clearly define the process for accurately improving blade health and structural robustness to withstand fatigue loads and maximum loads.

Figure 9 illustrates the complete assembly of the experimental test bench. The setup comprises several modules, including a base unit

embedding the blade, a motion transformation system actuated by a motor-reducer, and a camera-based monitoring system. Indeed, damage was monitored using a high-speed camera system with a resolution of 1920×1080 pixels and a frame rate of 500 fps, while image-processing techniques, including edge detection and thresholding, could be applied to identify cracks and delaminations. However, in the present study, damage detection was performed manually by visual inspection of images or video frames. The figure demonstrates the operation of the test bench under fatigue loading applied in the flapwise direction. The design and configuration of the setup are tailored to replicate realistic operating conditions and enable detailed damage monitoring throughout the testing procedure.

As illustrated in Fig. 10, fatigue tests revealed the formation of a critical buckling zone, as detected by the camera, characterized by pronounced local deformation induced by compressive forces resulting from the flexural shape of the structure. Truly, for future work, an acoustical study is proposed to detect first-ply failure and other damage mechanisms. This observation was in strong agreement with the numerical predictions obtained via buckling analysis in [28]; therefore, it validates the simulation model.

Figure 11 presents stiffness degradation measurements obtained from three different points on the blade in the flapwise and edgewise directions, with error bars illustrating the variability and uncertainty of the apparent bending stiffness over the course of the applied loading cycles. The results clearly indicate a significant reduction in flexural rigidity in the edgewise direction compared to the flapwise direction, accompanied by a reduction in material stiffness and an increase in total deformation energy. This anisotropic stiffness degradation highlights the importance of directional analysis in blade fatigue studies. Furthermore, Fig. 12 shows the evolution of damage near the blade root, where the stiffness loss at the first stage reached approximately 35% at 44k cycles, in stark contrast to the measurements taken near the blade tip. Subsequently, the stiffness drop reached approximately 77% at 100k cycles, with a corresponding decrease in stiffness of about 12% in the edgewise direction. In practice, damage mechanisms such as fiber breakage with moderate propagation justified the reduction in material stiffness and total deformation energy.

The stiffness loss at the first stage was mainly associated with delamination and matrix cracking, explaining the moderate reduction in stiffness. At the second stage, a significant reduction in stiffness and total deformation energy was observed, corroborated by the occurrence of fiber breakage with moderate propagation.

The damage propagation was further documented through high-resolution video capture. Matrix crushing was observed to initiate after approximately 35,000 cycles, followed by delamination and matrix cracking around 40,000 cycles. Fiber rupture was detected after 100,000 cycles, accompanied by progressive crack propagation, as evidenced in Fig. 12. After the onset of matrix damage and delamination and before the breakage of the first fiber, the stiffness of the structure was mainly influenced in both directions. The total deformation energy was related to the material stiffness and could be considered a relevant factor for assessing the rigidity of the blade structure. Thus, after fiber breakage, the structure partially recovered its flexural rigidity, with only a small percentage variation in degradation. Regarding the response of the composite blade, the mechanical interpretation is strengthened by explicitly correlating the observed stiffness degradation and the increase in deformation energy with the

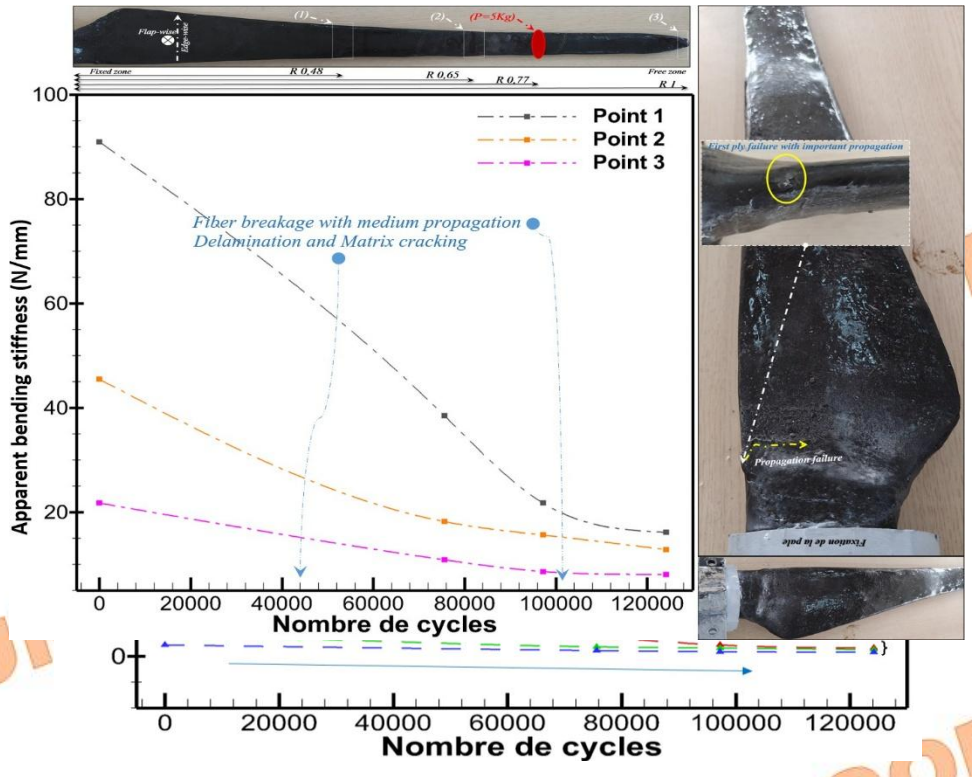

Fig. 11: Evolution of blade structural stiffness and total deformation energy during fatigue testing for different flexural directions; error bars indicate the variability of the measured values obtained from repeated measurements.

underlying damage mechanisms. Specifically, matrix cracking, delamination, and fiber breakage contribute to local reductions in stiffness and corresponding increases in deformation energy. These correlations are highlighted and illustrated in Figures 11 and 12, providing a clearer link between the mechanical response and the progressive damage observed during fatigue testing.

Mechanical testing of composite blades is an essential step in the certification process, ensuring that the blades meet strength and durability requirements under both static and dynamic loads. These evaluations also provide insight into the fatigue lifespan of the blade, as well as the stiffness degradation and damage progression over time. Numerous experimental campaigns have been carried out to assess the behavior of composite materials used in wind turbine blades, with the ultimate goal of optimizing blade geometry and load-bearing capacity.

In the current study, the blade's structural performance under cyclic fatigue was examined using the custom-built test bench. The test emphasized flapwise loading to investigate stiffness reduction. The findings reveal that the blade structure retained most of its stiffness over 60,000 cycles, with only marginal losses. However, localized damage, such as microcracking and delamination, was observed at the leading edge, contributing to structural weakening. These regions were therefore identified as critical zones requiring potential reinforcement.

To mitigate the observed damage and enhance mechanical resistance, it is proposed to integrate additional composite layers specifically in the regions subjected to severe stress concentrations. The orientation of these reinforcements should follow the direction of internal forces, thereby optimizing load transfer and improving fatigue resistance. Additive manufacturing techniques, including 3D printing, can be leveraged for the efficient fabrication of complex, reinforced geometries, allowing for faster prototyping and reduced production costs.

Continual iterative testing remains fundamental in refining blade designs for large-scale manufacturing. The strategy involves subjecting prototype blades to harsh environmental simulations in the principal direction, flapwise, to thoroughly assess fatigue tolerance and predict service life.

Ultimately, the experimentally identified damage zones substantially contribute to the overall stiffness degradation of the structure. This underscores the need to enhance resistance by strategically incorporating reinforcement layers in these critical regions. The progression observed in the structural damage is predominantly unidirectional, offering guidance

Fig.12: Reduction in local structural stiffness of the specimen following fatigue testing, highlighting the effects of matrix cracking, delamination, and fiber breakage on different regions of the structure.

for reinforcement orientation in future designs. Aligning fibers with the direction of internal forces, as suggested in [28, 30, 54], could significantly improve the structural performance of the blade under cyclic loading.

3.2. Uncertainty and repeatability analysis of experimental results

In this section, a comprehensive analysis is carried out to quantify measurement variability, evaluate statistical consistency, and guarantee the reliability of the experimental stiffness results. To ensure a high level of accuracy and reliability, a statistical analysis was performed for the measured stiffness of the blade prototypes. Each configuration was tested twice using two blades manufactured with identical materials and processing conditions. The outcomes of the statistical analysis include mean values, standard deviations, combined uncertainties, and coefficients of variation for the blade stiffness measurements.

The stiffness of the two wind turbine blade prototypes was measured at three points along the blade under cyclic loading (applied load P = 48.3 N, frequency f = 290 rad/s). The applied loading depends on the position of the slider, as illustrated in Fig. 9, where the slider was fixed at a single position. Each measurement was repeated twice for each prototype to assess and quantify the two analyses. Error propagation was applied for derived quantities, such as stiffness calculated as $k = P/\delta$.

Table 4 reports the raw stiffness evolution at the three measurement points. These data constitute the foundation for the subsequent analysis. At Point 1, a significant decrease in stiffness is observed after 80,000 cycles for both blades, indicating that this location is the most sensitive to fatigue-induced degradation. At Point 2, the absolute stiffness values are lower than at Point 1, and both blades exhibit a comparable monotonic decrease with fatigue, confirming consistent behavior at this intermediate span position. Accordingly, at Point 3, this location shows the lowest stiffness levels, as expected near the blade tip, but the differences between the two blades remain minimal, reflecting manufacturing uniformity.

The following tables provide the statistical treatment of the raw stiffness data. For each point and loading cycle, the following indicators are computed: mean stiffness. $\bar{k}$, standard deviation s, Type-A uncertainty u_A, Type-B instrument uncertainty u_B, combined standard uncertainty uc, and the coefficient of variation (CV). These quantities allow assessment of the repeatability of the measurements and the overall measurement uncertainty.

In practice, Tab. 5 reports the processed statistical metrics for Point 1. The standard deviation and Type-A uncertainties remain small relative to the mean stiffness, and the CV remains below 3.5%. Therefore, the combined uncertainty u_c confirms the reliability of the measurements even under significant stiffness degradation. Assumption: instrument (Type-B) standard uncertainty u_B = 0.20 kN/m. Hence, Table 6 summarizes the statistical indicators for Point 2. The uncertainty values remain nearly constant across fatigue states, and the CV stays below 3.3%, demonstrating strong results.

Therefore, Table 7 displays the statistical results for Point 3. The uncertainty levels are the lowest among all positions, with CV values consistently below 3%, indicating good results, particularly near the blade tip.

The complete statistical analysis confirms that the measurement procedure provides highly repeatable stiffness results across the three measurement points. Hence, the standard deviations and Type-A uncertainties remain small relative to the mean stiffness, and the CV always stays below 3.5%, indicating low dispersion. Consequently, the combined uncertainty u_c is primarily influenced by the assumed instrument uncertainty u_B, particularly when the measured variability is minimal. Overall, the results demonstrate excellent measurement reliability and confirm that the observed stiffness degradation with fatigue cycles corresponds to genuine structural behavior rather than measurement noise.

Based on all the processed tables above, the study for each measurement point can be summarized as follows. Key observations:

- **Repeatability**: Sample standard deviations s and Type-A uncertainties u_A are small relative to the mean stiffness, indicating good results between the two tested prototypes.

Table 4: Measured stiffness values (kN/m) of two blade prototypes at three measurement points for different fatigue cycles (Flap-wise direction)

Cycles	Point 1 (Blade 1)	Point 1 (Blade 2)	Point 2 (Blade 1)	Point 2 (Blade 2)	Point 3 (Blade 1)	Point 3 (Blade 2)
0	90	88	45	46	22	21.5
80,000	40	42	22	21	12	12.5
100,000	25	26	20	19.5	10	9.8
120,000	20	19.5	15	14.8	9.5	9.3

Table 5: Processed statistical results for Point 1 (kN/m)(Notes: $\bar{k}$is the mean stiffness, $s$the sample standard deviation, $u_A$the Type-A uncertainty (Eq. 10), $u_B$the assumed Type-B (instrument) uncertainty, and $u_c = \sqrt{u_A^2 + u_B^2}$ the combined uncertainty.)

Cycles	Mean ($\bar{k}$)	Standard Deviation (s)	Type-A Uncertainty (u_A)	Type-B Uncertainty (u_B)	Combined Uncertainty (u_c)	CV (%)
0	89.00	1.414	1.000	0.20	1.020	1.59
80,000	41.00	1.414	1.000	0.20	1.020	3.45
100,000	25.50	0.707	0.500	0.20	0.538	2.77
120,000	19.75	0.354	0.250	0.20	0.320	1.79

Table 6: Processed statistical results for Point 2 (kN/m)

Cycles	$\bar{k}$	s	u_A	u_B	u_c	CV (%)
0	45.50	0.707	0.500	0.20	0.539	1.55
80,000	21.50	0.707	0.500	0.20	0.539	3.29
100,000	19.75	0.354	0.250	0.20	0.320	1.79
120,000	14.90	0.141	0.100	0.20	0.224	0.95

Table 7:Processed statistical results for Point 3 (kN/m)

Cycles	$\bar{k}$	s	u_A	u_B	u_c	CV (%)
0	21.75	0.354	0.250	0.20	0.320	1.63
80,000	12.25	0.354	0.250	0.20	0.320	2.89
100,000	9.90	0.141	0.100	0.20	0.224	1.42
120,000	9.40	0.141	0.100	0.20	0.224	1.50

- **Measurement uncertainty**: With the assumed instrument uncertainty u_B = 0.20 kN/m, combined standard uncertainty u_c is dominated by u_B for points with small u_A, whereas in some cycles (e.g., early cycles at Point 1) u_A is comparable to u_B.
- **Coefficient of variation**: CV values are below 3.5% for all entries, confirming low relative dispersion and reliable measurements.
- **Fatigue trend**: Stiffness decreases with cycle count across all points; the statistical treatment confirms this is a real effect rather than measurement noise.

The assumed u_B can be adjusted according to the calibration values specific to your instruments; if exact calibration uncertainties were provided, the u_c values would be recomputed and updated in the tables.

The analysis demonstrates excellent results and low measurement uncertainty. Differences between the two blade prototypes were small (≤2 kN/m), Type-A uncertainties were low (≤0.7 kN/m), and CVs remained below 2% across all points and cycles. Combined uncertainty was dominated by instrument-related contributions (Type B), resulting in u_c ≈0.21–0.22 kN/m. Reporting the stiffness as $\bar{k} \pm u_c$ provides a reliable and transparent representation of experimental results and clearly highlights fatigue-induced stiffness degradation along the blade.

To complement the statistical analysis of the raw stiffness data, the propagation of uncertainty was evaluated for the first measurement point (Point 1). This analysis considers both uncorrelated and correlated contributions of the primary measured variables: applied load F and displacement δ, using Eqs. (11a) and (11b). The resulting uncertainties provide insight into the reliability of the stiffness measurements under fatigue loading.

Table 8 presents a representative set of propagated uncertainties at Point 1 for four fatigue states. Both uncorrelated and correlated propagation methods are shown, highlighting the impact of potential correlations between load and displacement measurements.

Table 8 shows that the propagated uncertainty decreases as the number of fatigue cycles increases. This trend is primarily due to the increasing displacement values with cycles, which reduce the sensitivity of stiffness to measurement errors in F and δ. The differences between the uncorrelated and correlated approaches are minor, indicating that the potential covariance between load and displacement measurements is relatively small. Overall, the propagated uncertainties are consistent with the Type-A and combined uncertainties reported previously (Tables 5–7), further confirming the reliability of the experimental stiffness measurements. The analysis demonstrates that, even under high fatigue levels, the experimental setup provides robust and quantitatively reliable stiffness data.

The propagated uncertainty for stiffness at Point 2 in Table 9 is slightly lower than at Point 1, reflecting smaller absolute stiffness values and moderate displacement magnitudes.

Actually, the propagated uncertainties at Point 2 are lower than at Point 1 and exhibit a decreasing trend with increasing cycle count. The difference between the uncorrelated and correlated propagation remains small, indicating limited covariance effects. These results confirm the good reliability of stiffness measurements at the midspan position of the blade.

Hence, Table 10 presents the propagated uncertainties for stiffness at Point 3, near the blade tip. This position exhibits the lowest absolute stiffness and the largest displacements, which reduce the relative impact of measurement uncertainties.

Thereby, the propagated uncertainty at Point 3 is the lowest among all positions, consistent with the larger displacements reducing stiffness sensitivity. Both the uncorrelated and correlated analyses yield nearly identical results, demonstrating minimal covariance effects. Overall, the uncertainty propagation analysis across all three points confirms the robustness of the experimental stiffness measurements under cyclic loading.

The total deformation energy of the blade structure, computed from the measured stiffness values at the three instrumented points, exhibits a clear increase with the number of fatigue cycles. This behavior reflects the progressive softening of the blade under cyclic loading. Among the measurement points, Point 3, located near the blade tip, accumulates the largest deformation energy, consistent with its lower stiffness and correspondingly higher deflection. Overall, the observed trend indicates that energy-based indicators provide a sensitive measure of damage accumulation and stiffness degradation, effectively capturing the structural deterioration of the blade throughout the fatigue tests. Truly, the literature [55, 56] proposes a nonlinear fatigue damage accumulation model based on the stiffness degradation pattern of composite laminates.

4. Conclusion

Careful attention has been paid to this experimental study, which investigated the mechanical performance of a segmented composite blade using a custom-built test bench. The blade was subjected to cyclic flapwise loading while its stiffness and local deformations were continuously monitored. The results showed a stiffness reduction of up to 77% at the root (Point 1) after 120,000 cycles, with corresponding decreases of 56% and 57% at Points 2 and 3, respectively.

Table 8:Propagated uncertainty in stiffness at Point 1 (kN/m)

Cycles	F (N)	δ (mm)	(u_k) (uncorrelated)	(u_k) (correlated)
0	48.3	0.537	1.02	1.05
80,000	48.3	1.18	1.02	1.04
100,000	48.3	1.90	0.54	0.56
120,000	48.3	2.44	0.32	0.33

Table 9:Propagated uncertainty in stiffness at Point 2 (kN/m)

Cycles	F (N)	δ (mm)	(uk) (uncorrelated)	(uk) (correlated)
0	48.3	1.06	0.54	0.56
80,000	48.3	2.25	0.54	0.55
100,000	48.3	2.42	0.32	0.33
120,000	48.3	3.24	0.22	0.23

Table 10:Propagated uncertainty in stiffness at Point 3 (kN/m)

Cycles	F (N)	δ (mm)	(u_k) (uncorrelated)	(u_k) (correlated)
0	48.3	2.25	0.32	0.33
80,000	48.3	4.03	0.32	0.33
100,000	48.3	4.83	0.22	0.23
120,000	48.3	5.13	0.21	0.22

Initial damage (matrix cracking and delamination) was observed after approximately 80,000 cycles, indicating critical zones susceptible to fatigue. The total deformation energy increased by 77.5% at the root, reflecting progressive softening of the structure.

Table 11:Total deformation energy U (J) at different measurement points and fatigue cycles

Cycles	Point 1	Point 2	Point 3
0	0.01295	0.0259	0.0530
80,000	0.0291	0.0530	0.0971
100,000	0.04662	0.05827	0.1165
120,000	0.05827	0.0777	0.1227

A statistical analysis confirmed valuable results, with coefficients of variation below 3.5% and combined measurement uncertainty under 10%, demonstrating that the observed stiffness degradation is a legitimate structural response rather than measurement noise.

Here, the main constraints of the present study were clearly discussed, including:

- Small-scale prototype effects, which may not fully reproduce the dynamic behavior of full-scale blades.
- Simplified internal structural configuration, which differs from industrial composite layups and may influence load transfer and damage initiation.
- Absence of environmental conditions, such as temperature, humidity, and UV exposure, which are known to affect composite fatigue behavior.
- Restricted number of specimens, limiting the statistical generalization of the findings.

These limitations will guide the next research steps, including full-scale investigations, environmental fatigue studies, and improved prototype manufacturing, using more advanced statistical analyses such as the Taguchi method or neural networks in modern artificial intelligence.

Nomenclature

C	Chord length (mm)
NACA	National Advisory Committee for Aeronautics
CATIA	Computer-Aided Three-Dimensional Interactive Application
3D Printing	Three-dimensional printing
HAWT	Horizontal Axis Wind Turbine
HAWTB	Horizontal Axis Wind Turbine Blade
AM	Additive Manufacturing
CFD	Computational Fluid Dynamics
RTM	Resin Transfer Molding
FEM	Finite Element Model
CV	Coefficient of Variation

Acknowledgments

This research was not supported by any public, commercial, or not-for-profit company.

Funding Statement

This research was not supported by any public, commercial, or not-for-profit company.

Conflicts of Interest

The authors declare that they have no conflict of interest.

References

[1] Zhang Hongjian, Xiaodong Liu, Cao Xinyu, Ningchuan Zhang, and Adrian Law. Assessment of structural stability and power performance for a novel hybrid wind-solar-wave energy system. Scientific Reports, 12 2025. Doi:10.1038/s41598-025-30805-9.

[2] Haytham Elmousalami, Aljawharah Alnaser, and Felix Hui. Sustainable AI-driven wind energy forecasting: advancing zero-carbon cities and environmental computation. Artificial Intelligence Review, 58, 03 2025. Doi:10.1007/s10462-025-11191-0.

[3] Fatima El Bakkari and Hamid Mounir. Compatible alternative energy storage systems for electric vehicles: Review of relevant technology derived from conventional systems. Energy, 288, 2024. DOI:10.1016/j.energy.2023.129775.

[4] Hamza Khaldi and Hamid Mounir. Comparative carbon footprint of electric and hydrogen vehicles: Insights from Morocco, Africa, and global energy transitions. Energy for Sustainable Development, 85, 2025. DOI:10.1016/j.esd.2025.101685.

[5] M Mansour, K Tsongas, D Tzetzis, and A Antoniadis. Mechanical and dynamic behavior of fused filament fabrication 3d printed polyethylene terephthalate glycol reinforced with carbon fibers. Polymer-Plastics Technology and Engineering, 57(16):1715–1725, 2018. DOI: 10.1080/03602559.2017.1419490.

[6] Y. Aydın, C. Cakiroglu, G. Bekdaş, and Z. W. Geem. Fatigue predictive modeling of composite materi-als for wind turbine blades using explainable gradient boosting models. Coatings, 15(3):325, 2025. DOI:10.3390/coatings15030325.

[7] Omar Rajad and Hamid Mounir. A review on the hawctb performance enhancement methods, numerical models and ai concept used for the blade composite structure assessment: Context of new industry 5.0. pages 1–6, Nov 2021. DOI:10.1109/IRSEC53969.2021.9741193.

[8] Ruixue Ji, Libin Zhao, Kangkang Wang, Fengrui Liu, Yu Gong, and Jianyu Zhang. Effects of debonding de-fects on the postbuckling and failure behaviors of composite stiffened panel under uniaxial compression. Composite Structures, 256, 2021. DOI:https://doi.org/10.1016/j.compstruct.2020.113121.

[9] Y. Bazilevs, K. Takizawa, E. Tezduyar, T. M.-C. Hsu, Y. Otoguro, H. Mochizuki, and C.H˜ . Wu, M.˙Ale and space–time variational multiscale isogeometric analysis of wind turbines and turbomachinery. page 195–233, 2020. DOI:10.1007/978-3-030-43736-77.

[10] S Fertahi, T Bouhal, Omar Rajad, T Kousksou, A Arid, T El Rhafiki, A Jamil, A Benbassou, et al. Cfd performance enhancement of a low cut-in speed current vertical tidal turbine through the nested hybridization of savonius and darrieus. Energy Conversion and Management, 169:266–278, 2018. DOI:https://doi.org/10.1016/j.enconman.2018.05.027.

[11] El-Harrach et al. An aerodynamic optimization approach for wind turbine blades using proper general-ized decomposition. Energies, 18(21):5846, 2025. DOI:10.3390/en18215846.

[12] Xiangrong Cheng, Bing Du, Jia He, Wanling Long, Guiyang Su, Jingwei Liu, Zhenhua Fan, and Liming Chen. A review of thermoplastic composites on wind turbine blades. Composites Part B: Engineering, 299:112411, 2025. DOI:https://doi.org/10.1016/j.compositesb.2025.112411.

[13] Sebastian Timme, Volker Trappe, Manfred Korzen, and Bernhard Schartel. Fire stability of carbon fiber reinforced polymer shells on the intermediate-scale. Composite Structures, 178(Supplement C):320 – 329, 2017. DOI:https://doi.org/10.1016/j.compstruct.2017.07.025.

[14] G. A. Carallo, M. Casa, C. Kelly, and M. Alsaadi. Comparative life cycle assessment (lca) of traditional and new sustainable wind blade construction. Sustainability, 17(5):2026, 2025. DOI:10.3390/su17052026.

[15] Ahmed Ali Geneid, Mostafa R. A. Atia, and Ahmed Badawy. Multi-objective optimization of vertical-axis wind turbine's blade structure using genetic algorithm. Journal of Engineering and Applied Science, 69, 2022. DOI:10.1186/s44147-022-00150-z.

[16] Xiao Chen, Philipp Ulrich Haselbach, Kim Branner, and Steen Hjelm Madsen. Effects of different material failures and surface contact on structural response of trailing

edge sections in composite wind turbine blades. Composite Structures, 226:111306, 2019. DOI:https://doi.org/10.1016/j.compstruct.2019.111306.

[17] Xiao Chen, Wei Zhao, Xiao Lu Zhao, and Jian Zhong Xu. Preliminary failure investigation of a 52.3m glass/epoxy composite wind turbine blade. Engineering Failure Analysis, 44:345–350, 2014. DOI:https://doi.org/10.1016/j.engfailanal.2014.05.024.

[18] Imane Amarir, Hamid Mounir, Omar Rajad, and Yassine Amadane. Fatigue performance investigation on the automotive welded structure under damped loads using the taguchi method. Heat Transfer, 52(1):162 – 192, 2023. DOI:10.1002/htj.22690.

[19] Anass Kheir, Hamid Mounir, Zakaria Lafdaili, Omar Rajad, and Ismail Lagrat. Modeling and analysis of lam-inate structures of a pressurized hydrogen tank. volume 469, 2023. DOI:10.1051/e3sconf/202346900022.

[20] Saïf ed Dîn Fertahi, T. Bouhal, A. Arid, T. Kousksou, A. Jamil, N. Moujibi, and A. Benbassou. Thermo-mechanical strength analysis for energy storage improvement of horizontal storage tanks integrating evacuated tube collectors. International Journal of Hydrogen Energy, 42(49):29370 – 29383, 2017. https://doi.org/10.1016/j.ijhydene.2017.10.016.

[21] Imane Amarir and Hamid Mounir. Experiment, simulation and investigation of the effect of different pa-rameters on the durability of welded structure under damped loads for automobile utilization. International Journal on Interactive Design and Manufacturing, 18(1):493 – 508, 2024. DOI:10.1007/s12008-023-01585-1.

[22] Imane Amarir and Hamid Mounir. Fatigue analysis case study of welded profiles for automotive utilization. IET Conference Proceedings, 2022(1):160 – 163, 2022. DOI:10.1049/icp.2022.0610.

[23] Saïf ed-Dîn Fertahi, Shafiqur Rehman, Ernesto Benini, Khadija Lahrech, Abderrahim Samaouali, Asmae Arbaoui, Imad Kadiri, and Rachid Agounoun. Insights from the last decade in computational fluid dy-namics (cfd) design and performance enhancement of darrieus wind turbines. Processes, 13(2), 2025. DOI:10.3390/pr13020370.

[24] Saïf ed-Dîn Fertahi, Shafiqur Rehman, Khadija Lahrech, Abderrahim Samaouali, Asmae Arbaoui, Imad Kadiri, and Rachid Agounoun. A review of comprehensive guidelines for computational fluid dynamics (cfd) validation in solar chimney power plants: Methodology and manzanares prototype case study. Fluids, 9(11), 2024. DOI:10.3390/fluids9110251.

[25] Z. Belfkira, H. Mounir, and A. El Marjani. Structural optimization of a horizontal axis wind turbine blade made from new hybrid composites with kenaf fibers. Composite Structures, 260:113252, 2021. DOI:https://doi.org/10.1016/j.compstruct.2020.113252.

[26] Xiao Chen, Peter Berring, Steen Hjelm Madsen, Kim Branner, and Sergei Semenov. Under-standing progressive failure mechanisms of a wind turbine blade trailing edge section through subcomponent tests and nonlinear fe analysis. Composite Structures, 214:422–438, 2019. DOI:https://doi.org/10.1016/j.compstruct.2019.02.024.

[27] Omar Rajad, Hamid Mounir, Abdellatif El Marjani, et al. Nonlinear modeling analysis of the coupled me-chanical strength and stiffness enhancement of composite materials of a horizontal axis wind turbine blade (hawtb). International Journal on Interactive Design and Manufacturing (IJIDeM), pages 1–24, 2022. DOI: https://doi.org/10.1007/s12008-021-00790-0.

[28] Omar Rajad, Hamid Mounir, and Abdellatif El Marjani. Modeling, understanding and enhancing the me-chanical response of the hawtb composite structure through the nonlinear fe analysis of a proposed sub-model. International Journal on Interactive Design and Manufacturing (IJIDeM), 15(4):631–659, 2021. DOI:https://doi.org/10.1007/s12008-021-00789-7.

[29] Jinghua Wang, Xuemei Huang, Chendi Wei, Leian Zhang, Chengliang Li, and Weisheng Liu. Failure analysis at trailing edge of a wind turbine blade through subcomponent test. Engineering Failure Analysis, page 105596, 2021. DOI:https://doi.org/10.1016/j.engfailanal.2021.105596.

[30] Zheng Liu, Jinlong Liang, Zhenfeng He, Xin Liu, Haodong Liu, and Zhenjiang Shao. A developed fatigue anal-ysis approach for composite wind turbine blade adhesive

joints using finite-element submodeling technique. Engineering Failure Analysis, 164:108701, 2024. DOI:https://doi.org/10.1016/j.engfailanal.2024.108701.

[31] Ismail Ezzaraa, Nadir Ayrilmis, Mohamed Abouelmajd, Manja Kitek Kuzman, Ahmed Bahlaoui, Ismail Ar-roub, Jamaa Bengourram, Manuel Lagache, and Soufiane Belhouideg. Numerical modeling based on fi-nite element analysis of 3d-printed wood-polylactic acid composites: A comparison with experimental data. Forests, 14(1), 2023. DOI:https://doi.org/10.3390/f14010095.

[32] César Balderrama-Armendáriz, Sergio Arbelaez-Rios, David Cortes, Jose Flores-Figueroa, Aide Maldonado, and Alberto Sierra. Optimizing the user experience of additive manufacturing products through material driven design. International Journal on Interactive Design and Manufacturing (IJIDeM), 19:5331–5346, 10 2024. DOI:10.1007/s12008-024-02131-3.

[33] Ashish Srivastava, Ajay Kumar, Parveen Kumar, Preeti Gautam, and Namrata Dogra. Research progress in metal additive manufacturing: Challenges and opportunities. International Journal on Interactive Design and Manufacturing (IJIDeM), pages 1–17, 12 2023. DOI:10.1007/s12008-023-01661-6.

[34] Marwane Rouway, Mourad Nachtane, Mostapha Tarfaoui, Nabil Chakhchaoui, L. Omari, Fouzia Fraija, and Omar Cherkaoui. 3d printing: rapid manufacturing of a new smallscale tidal turbine blade. The International Journal of Advanced Manufacturing Technology, 115, 07 2021. DOI:10.1007/s00170-021-07163-7.

[35] Andrés F. Olivera, Edwin Chica, and Henry A. Colorado. Design and manufacturing with 3d printing and life cycle analysis of a recyclable polymer-based h-darrieus wind turbine. Engineered Science, 31:1156, 2024. DOI:10.30919/es1156.

[36] SeokKoo Kang, Youngkyu Kim, Jiyong Lee, Ali Khosronejad, and Xiaolei Yang. Wake in-teractions of two horizontal axis tidal turbines in tandem. Ocean Engineering, 254, 2022. DOI:https://doi.org/10.1016/j.oceaneng.2022.111331.

[37] Imane Amarir, Hamid Mounir, Omar Rajad, and Yassine Amadane. Fatigue performance investigation on the automotive welded structure under damped loads using the taguchi method. Heat Transfer, 52(1):162–192, 2023. DOI:https://doi.org/10.1002/htj.22690.

[38] KK Guduru and Gangi Setti Srinivasu. 3d printed carbon fiber reinforced pla composite using fused de-position modeling by taguchi's optimization: influence of printing parameters. International Journal on Interactive Design and Manufacturing (IJIDeM), 19:3921–3931, 08 2024. DOI:10.1007/s12008-024-02040-5

[39] Marwane Rouway, Mostapha Tarfaoui, Nabil Chakhchaoui, Lhaj El Hachemi Omari, Fouzia Fraija, and Omar Cherkaoui. Additive manufacturing and composite materials for marine energy: Case of tidal turbine. 3D Printing and Additive Manufacturing, 10(6):1309–1319, 2023. DOI:10.1089/3dp.2021.0194.

[40] M. Tarfaoui, O. R. Shah, and M. Nachtane. Design and Optimization of Composite Offshore Wind Turbine Blades. Journal of Energy Resources Technology, 141(5), 01 2019. DOI:10.1115/1.4042414.

[41] T.Y. Kam, H.M. Su, and C.Y. Huang. Quasi-static buckling and first-ply failure loads of shear web rein-forced glass-fabric composite wind blades. Composite Structures, 160(Supplement C):1225 – 1235, 2017. DOI:https://doi.org/10.1016/j.compstruct.2016.10.087.

[42] Iec 61400-1: Wind energy generation systems — part 1: Design requirements.2019.https://webstore.iec.ch/en/publication/26423.

[43] Germanischer-lloyd (gl) design standard, guideline for the certification of wind turbines edition. guideline for onshore wind-turbine certification; in force since 1 july 2010. hamburg, germany. url:https://compositeskn.org/kpc/reference:b25f3c56-2083-36b5-9d1a-8bc33a6b1e24. 2010.

[44] T. Babu, A. Kowser, and A.N.M. Islam Mukut. Numerical investigation of wind turbine blade materials and airfoil profiles to extract maximum wind energy. International Journal for Simulation and Multidisciplinary Design Optimization, 15:25, 2024. DOI:10.1051/smdo/2024023.

[45] O. Rajad, M. Hamid, S. e. Fertahi, and A. E. Marjani. Fiber orientation effect on the behavior of the composite materials of the horizontal axis wind turbine blade (hawtb).

pages 1–6, 2018. DOI:10.1109/IRSEC.2018.8702930.

[46] Zhu Y. Lou L. Zhou A. Ma Y. Sun J. Zhao, S. Comparison and analysis of major research methods for non-destructive testing of wind turbine blades. Review of Scientific Instruments, 96:062001, 2025. DOI:10.1063/5.0252130.

[47] Airfoil tools,http://airfoiltools.com. 2022.

[48] Yunjung Jang, Hakgeun Kim, and Kiweon Kang. Progressive failure analysis for 5 mw-class wind turbine composite blades with debonding damage based on czm method. Applied Sciences, 12(24):12973, 2022. DOI:10.3390/app122412973.

[49] O. Rajad and H Mounir. The stiffness assessment of the blade composite structure using a pro-posed sub-model arbitrary rectangular with delamination effect. Int J Interact Des Manuf, 2022. DOI:https://doi.org/10.1007/s12008-022-00891-4.

[50] Miguel A. Valdivia-Camacho, Sergio Lopez Dubon, Fergus Cuthill, Marek J. Munko, Edward D. McCarthy, Parvez Alam, and Conchúr M. O' Brádaigh. Clamping parameters in full-scale tidal turbine blade tests: A case study. Ocean Engineering, 327:120722, 2025. DOI:https://doi.org/10.1016/j.oceaneng.2025.120722.

[51] Luca Bernardini, Mark O. McLinden, Xiaoxian Yang, and Markus Richter. How accurate are your experi-mental data a more accessible gum-based methodology for uncertainty evaluation. International Journal of Thermophysics, 45, 2024. DOI:10.1007/s10765-024-03446-9.

[52] M. Tao, S. Ren, and C. Lao. Overview and comparison of common measurement uncertainty eval-uation methods. Metrology Science and Technology, 68(6):40–48, 2024. DOI:10.12338/j.issn.2096-9015.2023.0263.

[53] N. Habibi, A. Jalid, A. Salih, and M. Es-sadek. Perpendicularity assessment and uncertainty estimation us-ing coordinate measuring machine. International Journal of Metrology and Quality Engineering, 14, 2023. DOI:10.1051/ijmqe/2023010.

[54] Omar Rajad, Hamid Mounir, Mohamed Rich, Soufiane Belhouideg, Chadia Haidar, and Amina El Kasri. Strength and stiffness characterization and enhancement of a horizontal axis wind turbine blade using an experimental fatigue test bench. International Journal on Interactive Design and Manufacturing (IJIDeM), 18(1):149–158, 2024. DOI:https://doi.org/10.1007/s12008-023-01434-1.

[55] Haixia Kou, Kongyuan Wei, Yanhu Liu, and Xuyao Zhang. Stiffness degradation modeling for composite wind turbine blades based on full-scale fatigue testing. Journal of Beijing Institute of Technology, 33(2):123–136, 2023. DOI:10.15918/j.jbit1004-0579.2022.126.

[56] Y. Wang, Z. Li, H. Zhou, and X. Chen. A common model for stiffness degradation of composites at material and product levels. Journal of Failure Analysis and Prevention, 23:1550–1557, 2023. DOI:10.1007/s11668-023-01692-x.